

FrequentNet : A New Deep Learning Baseline for Image Classification

Yifei Li¹ Zheng Wang² Kuangyan Song³ Yiming Sun⁴

Abstract

In this paper, we generalize the idea from the method called "PCANet" (Chan et al., 2015) to achieve a new baseline deep learning model for image classification. Instead of using principal component vectors as the filter vector in "PCANet", we use basis vectors in discrete Fourier analysis and wavelets analysis as our filter vectors. Both of them achieve comparable performance to "PCANet" in benchmark datasets. It is noticeable that our algorithms do not require any optimization techniques to get those basis.

1. Introduction

Convolutional Neural Networks(CNN)(Jarrett et al., 2009) has achieved tremendous success in image classification (Krizhevsky et al., 2012), and filter vectors in the network aim to capture different patterns of images. But in order to get those filter vectors, we need to resort to back-propagation to solve a complicated optimization problem. (Chan et al., 2015) Proposed a baseline model for image classification which does not require any kind of back propagation to learn the filter vector. Instead, they proposed to use left eigen-vectors of stacked images which is commonly known as principal component analysis (PCA) to be the filter vectors. This stems from the eigen-decomposition where we can decompose the target onto the orthogonal basis (eigen-vectors) from PCA. Projection along each orthogonal basis can represent certain patterns in the image. However, getting those eigen-vectors is time consuming, especially for large datasets even if some randomized algorithms (Halko et al., 2011) are applied. In the classical computer vision literature, researchers have developed multi-scaled representation of images without resorting to optimization. Two most widely used ones are Discrete Fourier Transformation(DFT) (Nordberg, 1995) and Wavelets analysis (Mallat, 1996). (Fan et al., 2018) also extend the framework of PCANet by a

¹Department of Computer Science, Zhejiang University
²Department of Computer Science, Tongji University
³Zshield Inc.
⁴AWS AI, Amazon. Correspondence to: Yiming Sun <ys784@cornell.edu>.

second-order pooling strategy. In this paper, we explore the possibility to use basis from DFT and Wavelets analysis as candidates for filter vectors. Before we present our algorithms, let us have a brief review of both Discrete Fourier Transformation and wavelets analysis.

1.1. Discrete Fourier Transformation

Discrete Fourier Transformation (DFT)(Beerends et al., 2003) can represent the information in image at different frequencies. Mathematically, given a vectorized image \mathbf{x} of length n , 1D DFT transforms it as $d(\omega_k) = \langle \mathbf{x}, (C(\omega_k) - iS(\omega_k)) \rangle$, $\omega_k = 2\pi k/n$, $k \in F_n$, the set of Fourier frequencies. To be precise, F_n denotes the set $\{-[\frac{n-1}{2}], \dots, [\frac{n}{2}]\}$ where $[x]$ is the integer part of x , where

$$\begin{aligned} C(\omega_k) &= \frac{1}{\sqrt{n}}(1, \cos \omega_k, \dots, \cos(n-1)\omega_k)^\top, \\ S(\omega_k) &= \frac{1}{\sqrt{n}}(1, \sin \omega_k, \dots, \sin(n-1)\omega_k)^\top. \end{aligned} \quad (1)$$

Researchers have found that different frequencies can capture different levels of information in the image. For example, the high-pass filter will only select high-frequency signals to get the structured information like edges, while low-pass filter will select low-frequency signals and thus generate an over-smoothed and blurry image. (Costen et al., 1996). There are many traditional models focused on the detection of high-frequency information. For example, typical gradient-based method like sobel operator (Gao et al., 2010), prewitt operator (Yang et al., 2011) and canny operator (Canny, 1986) detect the high-frequency information in 1-order gradient domain. The laplacian operator (Wang, 2007) focuses on the 2-order gradient, which was widely used in image processing to sharpen the image. We refer (Kumar et al., 2013) for interesting readers to get a comprehensive understanding of edge detectors in image processing. In this work, we mainly focuses on the discrete Fourier transformation, since it has simpler form and can be easily extended to convolutional filters.

1.2. Wavelets Analysis

Different from DFT, wavelets aim to implement spectral analysis locally in the graph. We applied Daubechies D4 Wavelet Transform (Strang & Nguyen, 1996) (later we call it

DB4) in our paper. In DB4, the first layer wavelets analysis can be taken as project the image vector \mathbf{x} onto filter vectors formed with progressive local basis vector as

$$\begin{aligned}\mathbf{h} &= \left[\frac{1+\sqrt{3}}{4}, \frac{3+\sqrt{3}}{4}, \frac{3-\sqrt{3}}{4}, \frac{1-\sqrt{3}}{4} \right] \\ \mathbf{g} &= \left[\frac{1-\sqrt{3}}{4}, \frac{\sqrt{3}-3}{4}, \frac{3+\sqrt{3}}{4}, \frac{-1-\sqrt{3}}{4} \right].\end{aligned}\quad (2)$$

\mathbf{h} is calculating the moving average, which performs as low pass filtering in above section, while \mathbf{g} is capturing the comparison of local graph performing as high pass filtering in above section. Then for vectorized image \mathbf{x} , the first layer wavelet is like linear transformation in for n filter vectors as

$$\begin{bmatrix} h_0 & h_1 & h_2 & h_3 & \cdots & \cdots & \cdots \\ g_0 & g_1 & g_2 & g_3 & \cdots & \cdots & \cdots \\ 0 & 0 & h_0 & h_1 & h_2 & h_3 & \cdots \\ 0 & 0 & g_0 & g_1 & g_2 & g_3 & \cdots \\ \vdots & \vdots & \vdots & \vdots & \vdots & \vdots & \ddots \end{bmatrix} \mathbf{x}. \quad (3)$$

In this case, we can treat each line of left matrix in (3) as the pool of our potential filter vectors.

2. FrequentNet

2.1. Problem Setup

In this section we mainly follow the settings in (Chan et al., 2015). Provided with N input training images, $\{\mathcal{I}_i\}_{i=1}^N$ of size $m \times n$ and we set the patch size (or 2D filter size) as $k_1 \times k_2$ at all stages. We call those vectorized patches $\mathbf{x}_{i,1}, \dots, \mathbf{x}_{i,mn}$ where the first index is for image and the second index is for patches. Then we subtract patch mean from each patch and obtain

$$\bar{\mathbf{X}}_i = [\mathbf{x}_{i,1}, \dots, \mathbf{x}_{i,j}, \dots, \mathbf{x}_{i,mn}], 1 \leq j \leq mn \quad (4)$$

of size $k_1 k_2 \times mn$. Then we stack $\bar{\mathbf{X}}_i$ again to get

$$\bar{\mathbf{X}} = [\bar{\mathbf{X}}_1, \dots, \bar{\mathbf{X}}_i, \dots, \bar{\mathbf{X}}_N], 1 \leq i \leq N. \quad (5)$$

Its size is $k_1 k_2 \times mnN$. Then filter vectors aim to find patterns that can represent information in columns in $\mathbf{x}_{i,j}$ effectively. PCANet chooses the filter vectors to be the top left eigen-vectors of $\bar{\mathbf{X}}$. In this paper, we proposed to use basis in DFT and wavelets. In order to maintain the same size of image, we set convolution stride to 1 and zero-pad each image before convolving with the learned frequent filters. The overall pipeline is same as PCANet, where a simple strategy like hashing and histogram is applied to obtain the final representation features.

2.2. FourierNet

The First Stage: To avoid duplicates in Fourier basis, we restrict the index k in ω_k within $k \in F_n^+$, where F_n^+

Algorithm 1 Select top K Fourier Basis

```

Input:  $\bar{\mathbf{X}}, L_1$ 
for  $k$  in  $F_{k_1 k_2}^+$  do
     $c_k \leftarrow \|\langle C(\omega_k), \bar{\mathbf{X}} \rangle\|_1$ 
     $s_k \leftarrow \|\langle S(\omega_k), \bar{\mathbf{X}} \rangle\|_1$ 
end for
Select  $C(\omega_k)$  or  $S(\omega_k)$  with top  $L_1$  largest values in  $\{s_k, c_k\}$  and call the set of  $\mathcal{D}_{L_1}$ 
Output:  $\mathcal{D}_{L_1}$ 

```

only contains non-negative indices in F_n . And we choose $\{\cos(\omega_k), \sin(\omega_k)\}$ to be our candidate orthogonal basis. We then select certain filters of different frequencies based on the magnitude of the inner product of vectorized patches $\mathbf{x}_{i,j}$ and candidate filters, as is summarized in Algorithm 1. With the obtained L_1 filters $\mathbf{v}_1, \dots, \mathbf{v}_k, \dots, \mathbf{v}_{L_1}$, every input image \mathcal{I}_i is mapped to L_1 new feature maps:

$$\mathcal{I}_i^k = \mathcal{I}_i * \text{mat}_{k_1, k_2}(\mathbf{v}_k), \quad (6)$$

where $*$ is the two dimensional convolution. For later convenience, we rank $\mathbf{v} \in \mathcal{D}_{L_1}$ reversely based on $\|\langle \mathbf{v}_1, \bar{\mathbf{X}} \rangle\|_1$ reversely and set index based on it, i.e., $\|\langle \mathbf{v}_1, \bar{\mathbf{X}} \rangle\|_1 \geq \dots \geq \|\langle \mathbf{v}_{L_1}, \bar{\mathbf{X}} \rangle\|_1$.

The Second Stage: After the first stage, for each basis in \mathcal{D}_{L_1} , we get a new set of feature maps of the same size as original images. For the new $L_1 N$ feature maps $\mathcal{I}_i^k, i = 1, \dots, N, k = 1, \dots, L_1$, we continue to collect all overlapping patches and subtract mean from them. Define

$$\bar{\mathbf{Y}}_i^k = [\mathbf{y}_{i,1}^k; \dots; \mathbf{y}_{i,mn}^k] \quad (7)$$

then we could concatenate all $\bar{\mathbf{Y}}_i^k$ and get

$$\bar{\mathbf{Y}} = [\bar{\mathbf{Y}}_1^1; \dots; \bar{\mathbf{Y}}_N^{L_1}] \quad (8)$$

of size $k_1 k_2 \times L_1 N mn$. For $\bar{\mathbf{Y}}$, we run Algorithm 1 again to select top L_2 Fourier basis and follow above definition, we call the basis $\mathbf{u}_1, \dots, \mathbf{u}_{L_2}$ based on the magnitude of the inner product.

Output Stage: At output stage, we use simple hashing and histogram to get the final feature vectors. Generally, we first binarize all feature maps, then group these feature maps by the parent feature maps. For example, \mathcal{I}_i^k is the parent feature maps of \mathcal{I}_i^l and \mathcal{I}_i^l is the parent feature map of $\{\mathcal{I}_i^k * \mathbf{v}_l\}$. Then in each group, we pool the corresponding feature maps channel-wise by an exponential function. This hashing and pooling operation will reduce the dimension of the feature representations while preserve significant discriminative information. Finally, in histogram stage, we again extract blocks by a sliding window and compute the histogram of each block. Then we simply concatenate these

histograms originated from one image as the final feature vector of this image.

Specifically, for the 1-stage FourierNet, we extract $NL1$ feature maps denoted as \mathcal{I}_i^k after the first stage. Then the feature maps are binarized and grouped by image index i , $\{\mathcal{I}_i^1, \dots, \mathcal{I}_i^{L_1}\}$ for example.

$$\mathcal{T}_i = \sum_{k=1}^{L_1} 2^{k-1} B(\mathcal{I}_i * \mathbf{v}_k) \quad (9)$$

For the 2-stage FourierNet, we extract $NL1L2$ feature maps denoted as $\{\mathcal{I}_i^k * \mathbf{v}_l\}$. Then these feature maps are binarized and grouped by image index i and stage-1 filters index k .

$$\mathcal{T}_i^k = \sum_{l=1}^{L_2} 2^{l-1} B(\mathcal{I}_i^k * \mathbf{u}_l) \quad (10)$$

After grouping, we pool the feature maps channel-wise and concatenate histogram vectors like aforementioned. In CIFAR10 experiments, we also use Spatial Pyramid Pooling(SPP) layer from (He et al., 2015) to decrease the length of feature vector as well as extract more robust features invariant to object poses, scales and colors etc.

2.3. WaveletsNet

For waveletsNet, the whole process is very similar to FourierNet, the only difference now is that now the pool of candidate filter vectors become all rows in (3). Again, for stage I, we select L_1 filter vectors again based on magnitude of inner product between filter vector and vectorized image vector. At the this point, we can either go to output stage, or further we repeat the the selecting procedure to further select L_2 filters and then go to the output stage.

3. Experiments

We evaluated and compared the performances of FourierNet, PCANet and RandNet on two tasks, the hand-written digits recognition and object recognition.

3.1. Hand-written Digits Recognition

The MNIST (LeCun et al., 1998) and MNIST variations (Larochelle et al., 2007) are common benchmarks for testing hierarchical representations (Chan et al., 2015). We pick a subset of MNIST and its variations to experiment on, as listed in Table 1.

3.1.1. EXPERIMENT SETUP

We investigated the impact of number of filters L_1 on the proposed structure using one stage structure. We fixed patch size to 7×7 and patch stride to 1. Other experiment settings for one stage structure are listed in Table 2. For two stages structure, we mainly compared the performances between model based on different basis vectors using the two stages

Table 1. Descriptions of MNIST and MNIST variations picked for experiment

Datasets	Description
MNIST	Standard MNIST
basic	A smaller subset of standard MNIST
bg-rand	MNIST with noise background
rot	MNIST with rotation
bg-img	MNIST with image background
bg-img-rot	MNIST with rotation and image background

Table 2. Experiment setup for one stage structures

Datasets	patch stride	block size	block stride
basic	1	7×7	3
bg-rand	1	4×4	2
rot	1	4×4	2
bg-img	1	4×4	2
bg-img-rot	1	4×4	2

structure. We follow the recommended configurations for different dataset in the original PCANet paper, which are listed in Table 3.

3.1.2. EXPERIMENT RESULTS

The testing accuracy of the one stage models on the selected datasets, with the number of filters varies from 2 to 8 are shown in Figure 2. We can see from the results that the testing accuracy increases when the number of filters grows. The testing results for the two stage models, with the key setup in Table 3 are listed in Table 4. One can see that FourierNet-2 and WaveNet-2 achieves similar testing accuracy on these datasets. We also listed the learned first and second stage fourier filters from the *bg-rand* dataset in Figure 1. In order to visualize the features captured by the learned filters, we selected two samples from MNIST dataset, then performed low rank approximation through convolution. Figure 3 shows the selected MNIST samples. Figure 4 shows the selected low rank approximations using

Table 3. Experiment setup for two stages structure

Datasets	L_1	L_2	patch size	patch stride	block size	block stride
basic	6	8	7×7	1	7×7	3
bg-rot	6	8	7×7	1	4×4	2
bg-rand	6	8	7×7	1	4×4	2
bg-img	6	8	7×7	1	4×4	2
bg-img-rot	6	8	7×7	1	4×4	2
cifar10	40	8	5×5	1	8×8	4

Table 4. Testing Accuracies(%) of different methods of MNIST and its variations

Methods	basic	bg-rand	rot	bg-img	bg-img-rot
FourierNet-2	98.05	90.50	89.45	86.55	60.25
FourierNet-1	98.75	89.95	85.15	85.45	49.65
WaveNet-2	98.55	88.05	83.60	84.45	49.25
WaveNet-1	97.55	83.60	83.60	78.05	42.20
PCANet-2	98.15	91.55	89.50	87.20	62.50
PCANet-1	98.65	91.80	87.35	86.65	54.35
RandNet-2	97.55	82.70	86.00	83.40	40.00
RandNet-1	97.95	70.90	77.55	67.55	29.90

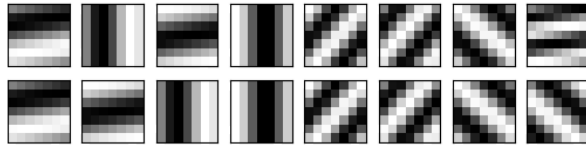


Figure 1. The fourier filters learned from *bg-rand* dataset. Top: the first stage filters. Bottom: the second stage filters.

filters from FourierNet, PCANet and RandomNet. More low rank approximations could be found in Appendix.

3.2. CIFAR10 Object Recognition

CIFAR10 contains 10 classes with 50000 training samples and 10000 test samples, which vary in object position, scale, colors and textures (Chan et al., 2015). We fix the number of filters in the first stage to 40, and the number of filters in second stage to 5. We also fix the patch size to 5×5 , block size to 8×8 and block overlap to 4. We tried different combinations of methods for the two stage structure. Specifically, Fourier-Fourier is simply FourierNet-2 where we use fourier filters for both stages, while Fourier-PCA means we use fourier filters for the first stage and PCA filters for the second stage. The rest combinations follow the definition similarly. The testing accuracy of different combinations are listed in Table 5. We also listed the learned filters of FourierNet-2 and PCANet-2 in Figure 6 and Figure 7 respectively.

Table 5. Testing accuracy(%) of different methods on CIFAR10

Methods	Accuracy
Fourier-Fourier	67.70
Fourier-PCA	68.30
PCA-Fourier	69.75
PCA-PCA	70.95

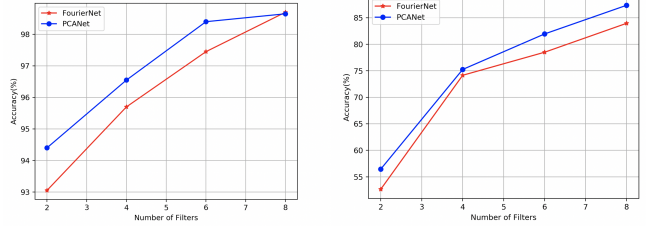


Figure 2. Test accuracy(%) of FourierNet-1 and PCANet-1 on MNIST basic and rot test set for varying number of filters(L_1). We tested L_1 varies from 2 to 8.

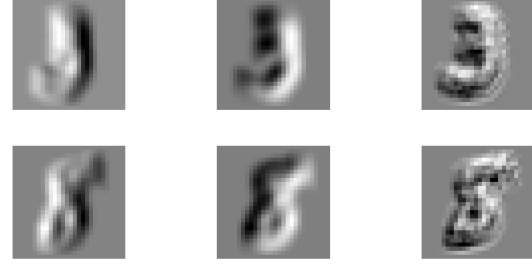


(a) Sample 1



(b) Sample 2

Figure 3. The selected two MNIST samples used for low rank approximation



(a) Fourier filter (b) PCA filter (c) Random filter

Figure 4. The low rank approximations of each type of selected filters for two samples from MNIST dataset, from left to right: (a) selected Fourier filter; (b) selected PCA filter; (c) selected Random filter. We picked one filter for each basis, then performed convolution over the 28×28 image samples.

4. Conclusion

In this paper, we proposed to use basis from Discrete Fourier Transformation and wavelets analysis to be the pool of potential filter vectors for selection. This procedure does not require any optimization and achieves comparable prediction accuracy to "PCANet". In the future, we will extend the basis to two dimensional Discrete Fourier Transformation and wavelets analysis (Alleyne & Cawley, 1991; Antoine et al., 2008). Lots of progresses has been made in neural network in graph (GNN) (Zhang et al., 2018), we also plan to extend our work to neural work in graph structure.

References

Alleyne, D. and Cawley, P. A two-dimensional fourier transform method for the measurement of propagating multimode signals. *The Journal of the Acoustical Society of America*, 89(3):1159–1168, 1991.

Antoine, J.-P., Murenzi, R., Vandergheynst, P., and Ali, S. T. *Two-dimensional wavelets and their relatives*. Cambridge University Press, 2008.

Beerends, R. J., ter Morsche, H. G., Van den Berg, J., and Van de Vrie, E. Fourier and laplace transforms. *Fourier and Laplace Transforms, by RJ Beerends and HG ter Morsche and JC van den Berg and EM van de Vrie*, pp. 458. ISBN 0521534410. Cambridge, UK: Cambridge University Press, August 2003., pp. 458, 2003.

Canny, J. A computational approach to edge detection. *IEEE Transactions on pattern analysis and machine intelligence*, (6):679–698, 1986.

Chan, T.-H., Jia, K., Gao, S., Lu, J., Zeng, Z., and Ma, Y. Pcanet: A simple deep learning baseline for image classification? *IEEE transactions on image processing*, 24(12):5017–5032, 2015.

Costen, N. P., Parker, D. M., and Craw, I. Effects of high-pass and low-pass spatial filtering on face identification. *Perception & psychophysics*, 58(4):602–612, 1996.

Fan, C., Hong, X., Tian, L., Ming, Y., Pietikäinen, M., and Zhao, G. Pcanet-ii: When pcanet meets the second order pooling. *IEICE TRANSACTIONS on Information and Systems*, 101(8):2159–2162, 2018.

Gao, W., Zhang, X., Yang, L., and Liu, H. An improved sobel edge detection. In *2010 3rd International Conference on Computer Science and Information Technology*, volume 5, pp. 67–71. IEEE, 2010.

Halko, N., Martinsson, P.-G., and Tropp, J. A. Finding structure with randomness: Probabilistic algorithms for constructing approximate matrix decompositions. *SIAM review*, 53(2):217–288, 2011.

He, K., Zhang, X., Ren, S., and Sun, J. Spatial pyramid pooling in deep convolutional networks for visual recognition. *IEEE transactions on pattern analysis and machine intelligence*, 37(9):1904–1916, 2015.

Jarrett, K., Kavukcuoglu, K., Ranzato, M., and LeCun, Y. What is the best multi-stage architecture for object recognition? In *2009 IEEE 12th international conference on computer vision*, pp. 2146–2153. IEEE, 2009.

Krizhevsky, A., Sutskever, I., and Hinton, G. E. Imagenet classification with deep convolutional neural networks. In *Advances in neural information processing systems*, pp. 1097–1105, 2012.

Kumar, M., Saxena, R., et al. Algorithm and technique on various edge detection: A survey. *Signal & Image Processing*, 4(3):65, 2013.

Larochelle, H., Erhan, D., Courville, A., Bergstra, J., and Bengio, Y. An empirical evaluation of deep architectures on problems with many factors of variation. In *Proceedings of the 24th international conference on Machine learning*, pp. 473–480. ACM, 2007.

LeCun, Y., Bottou, L., Bengio, Y., Haffner, P., et al. Gradient-based learning applied to document recognition. *Proceedings of the IEEE*, 86(11):2278–2324, 1998.

Mallat, S. Wavelets for a vision. *Proceedings of the IEEE*, 84(4):604–614, 1996.

Nordberg, K. Fourier transforms. 1995.

Strang, G. and Nguyen, T. *Wavelets and filter banks*. SIAM, 1996.

Wang, X. Laplacian operator-based edge detectors. *IEEE Transactions on Pattern Analysis and Machine Intelligence*, 29(5):886–890, 2007.

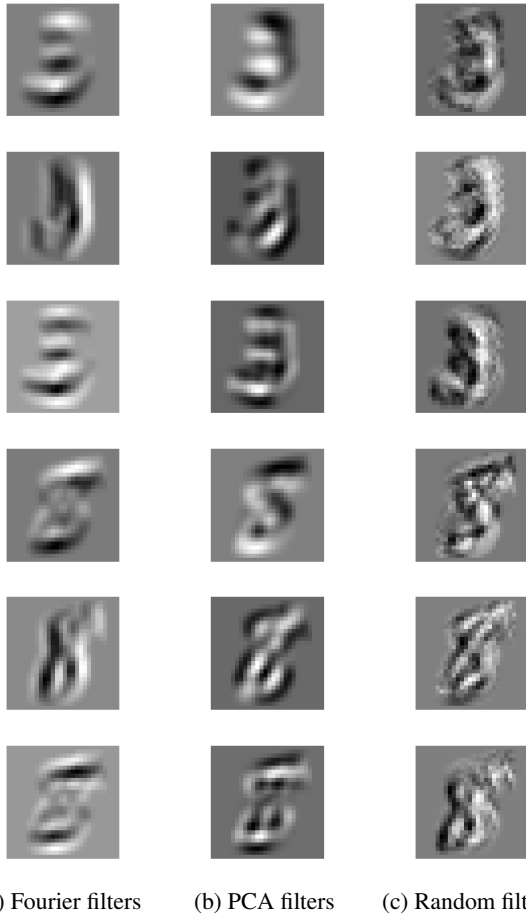
Yang, L., Wu, X., Zhao, D., Li, H., and Zhai, J. An improved prewitt algorithm for edge detection based on noised image. In *2011 4th International Congress on Image and Signal Processing*, volume 3, pp. 1197–1200. IEEE, 2011.

Zhang, Z., Cui, P., and Zhu, W. Deep learning on graphs: A survey. *arXiv preprint arXiv:1812.04202*, 2018.

5. Appendix

5.1. More low rank approximations

We present more low rank approximations here, each image in Figure 5 represents one low rank recovered MNIST sample.



(a) Fourier filters (b) PCA filters (c) Random filters

Figure 5. More recovered MNIST samples of selected filters, from left to right: (a)Low rank approximations using Fourier filters; (b)Low rank approximations using PCA filters; (c)Low rank approximations using Random filters

5.2. Visualization of filters of FourierNet and PCANet learned from CIFAR10 dataset

The learned filters of FourierNet-2 and PCANet-2 on *CIFAR10*. We visualize the

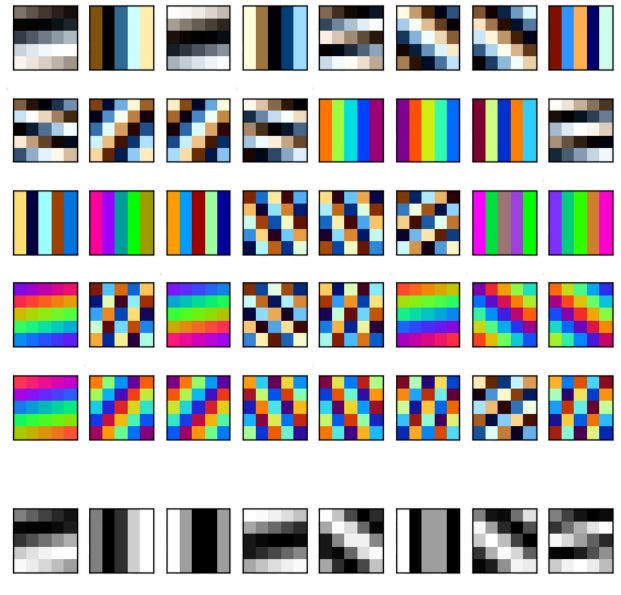


Figure 6. The fourier filters learned from *CIFAR10* dataset. Top: the first stage filters, we set the number of filters for each channel to 40. Bottom: the second stage filters, the number of filters are set to 8.

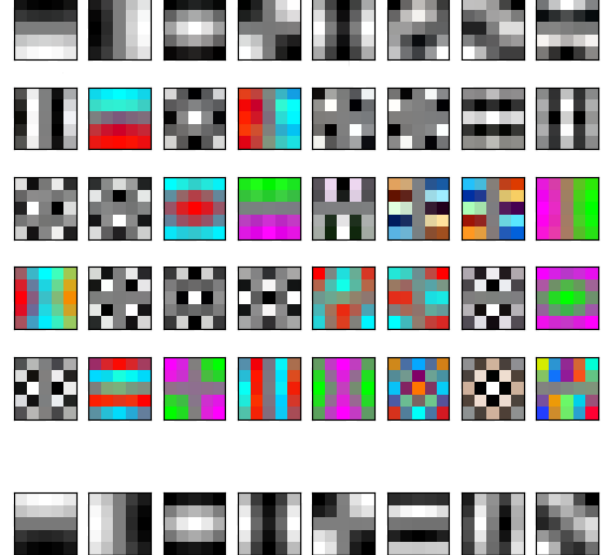


Figure 7. The PCA filters learned from *CIFAR10* dataset. Top: the first stage filters, the number of filters for each channel is 40. Bottom: the second stage filters, the number of filters is 8.